

12-1-2021

A detailed hydrothermal investigation of a helical micro double-tube heat exchanger for a wide range of helix pitch length

Nidal H. Abu-Hamdeh
King Abdulaziz University

Radi A. Alsulami
King Abdulaziz University

Muhyaddin J.H. Rawa
King Abdulaziz University

Abdulmalik A. Aljinaidi
King Abdulaziz University

Mashhour A. Alazwari
King Abdulaziz University

See next page for additional authors

Follow this and additional works at: https://digitalcommons.fiu.edu/all_faculty

Recommended Citation

Abu-Hamdeh, Nidal H.; Alsulami, Radi A.; Rawa, Muhyaddin J.H.; Aljinaidi, Abdulmalik A.; Alazwari, Mashhour A.; Eltahir, Mohamed A.; Almitani, Khalid H.; Alnefaie, Khaled A.; Abusorrah, Abdullah M.; Sindi, Hatem F.; Goodarzi, Marjan; and Safaei, Mohammad Reza, "A detailed hydrothermal investigation of a helical micro double-tube heat exchanger for a wide range of helix pitch length" (2021). *All Faculty*. 263. https://digitalcommons.fiu.edu/all_faculty/263

This work is brought to you for free and open access by FIU Digital Commons. It has been accepted for inclusion in All Faculty by an authorized administrator of FIU Digital Commons. For more information, please contact dcc@fiu.edu.

Authors

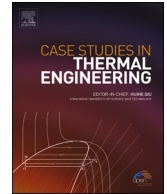
Nidal H. Abu-Hamdeh, Radi A. Alsulami, Muhyaddin J.H. Rawa, Abdulmalik A. Aljinaidi, Mashhour A. Alazwari, Mohamed A. Eltaher, Khalid H. Almitani, Khaled A. Alnefaie, Abdullah M. Abusorrah, Hatem F. Sindi, Marjan Goodarzi, and Mohammad Reza Safaei



ELSEVIER

Contents lists available at ScienceDirect

Case Studies in Thermal Engineering

journal homepage: www.elsevier.com/locate/csite

A detailed hydrothermal investigation of a helical micro double-tube heat exchanger for a wide range of helix pitch length

Nidal H. Abu-Hamdeh^a, Radi A. Alsulami^b, Muhyaddin J.H. Rawa^c,
 Abdulmalik A. Aljinaidi^b, Mashhour A. Alazwari^b, Mohamed A. Eltaher^b,
 Khalid H. Almitani^b, Khaled A. Alnefaie^b, Abdullah M. Abusorrah^c, Hatem F. Sindi^c,
 Marjan Goodarzi^{d,e,g,*}, Mohammad Reza Safaei^{b,f}

^a Center of Research Excellence in Renewable Energy and Power Systems, and Department of Mechanical Engineering, Faculty of Engineering, K. A. CARE Energy Research and Innovation Center, King Abdulaziz University, Jeddah, Saudi Arabia

^b Mechanical Engineering Department, Faculty of Engineering, King Abdulaziz University, Jeddah, 21511, Saudi Arabia

^c Center of Research Excellence in Renewable Energy and Power Systems, Department of Electrical and Computer Engineering, Faculty of Engineering, King Abdulaziz University, Jeddah, 21589, Saudi Arabia

^d Department of Mathematics, Faculty of Science, King Abdulaziz University, P.O. Box 80259, Jeddah, Saudi Arabia

^e Department of Medical Research, China Medical University Hospital, China Medical University, Taichung, Taiwan

^f Department of Mechanical Engineering, Florida International University, Miami, FL, 33174, USA

^g Mechanical Engineering Department, Lamar University, Beaumont, TX 77706, USA

ARTICLE INFO

Keywords:

Helical heat exchanger
 Microtube
 Heat transfer
 Finite volume method
 Secondary flow

ABSTRACT

The present study was numerically inquired the heat transfer performance and fluid flow characteristic of a helical micro double-tube heat exchanger (HMDTHX) using the finite volume method. The tube length was considered to be constantly equal to 30 mm, and 12 different configurations were modeled by changing in turn number and pitch length (P) for Reynolds numbers of 50, 100, 150, and 200. The findings indicated that the heat transfer would enhance by applying any helix angle in the straight tube. However, it had an optimum point which varied by Reynolds number (Re). Rising Re caused overall heat transfer coefficient (OHTC), pressure drop, and pumping power augment for all cases. Increasing P in overall reduced OHTC, pressure drop, and pumping power which had different maximum points between $P = 0.5$ to 3. Maximum overall heat transfer coefficient (OHTC) enhancement was equal to 45% for $Re = 200$ and $P = 2$. Also, maximum effectiveness was 11.5% for $P = 2$ and $Re = 200$. Moreover, a 42% maximum increment was achieved for pressure drop, pumping power, and friction factor at $Re = 200$ and $P = 2$. Shear stress for $Re = 100$ to 200 showed that the values are almost the same for $P = 0.5$ and 1. Then by increasing P, the shear stress decreases. While, for $Re = 50$, a maximum is seen at $P = 2$. The temperature distribution was indicated that the maximum temperature of the straight tube and helical tube are the same, but the difference is in the average temperature, which was 3.2 K between straight and helical tubes. Finally, by investigating the velocity contour, it was determined that a secondary flow through the HMDTHX, affected by centrifugal force, was existed, enhancing the fluid flow turbulency and heat transfer rate.

* Corresponding author. Mechanical Engineering Department, Lamar University, Beaumont, TX, 77706, USA.
 E-mail address: mgoodarzi@lamar.edu (M. Goodarzi).

<https://doi.org/10.1016/j.csite.2021.101413>

Received 5 August 2021; Received in revised form 29 August 2021; Accepted 31 August 2021

Available online 3 September 2021

2214-157X/© 2021 The Authors. Published by Elsevier Ltd. This is an open access article under the CC BY license

(<http://creativecommons.org/licenses/by/4.0/>).

1. Introduction

Since heat exchangers (HXs) have high application in industrial plants, their performance has been increasingly investigated by researchers from various sciences [1,2]. In this way, a compound technique should be applied to a study to warrant an efficient heat transfer improvement. It is figured with active, passive, and other techniques [3–5]. Using nanoparticles in working fluid or fluid

Nomenclature

A	Surface area (m^2)
C_p	Specific heat capacity ($J/kg K$)
C_{min}	Minimum water's heat capacity
d_i	Inner diameter of the tube side (μm)
d_o	Inner diameter of the shell tube (μm)
f	Friction factor
D	Diameter (mm)
n	Turns number
P	pitch length (mm)
H	Length (mm)
h	Heat transfer coefficient ($W/m^2 K$)
L	The length of the heat exchanger (mm)
\dot{m}	Mass flow rate (Kg/s)
p	Pressure (Pa)
P_p	Pumping power (W)
q	Input heat flux (W/m^2)
q_{max}	Maximum heat received (W)
Q_{abs}	Heat received by water (W)
r	Radius of tube side (mm)
T	Temperature (K)
HMDTHX	Helical micro double-tube heat exchanger
V	Velocity (m/s)

Greek symbol

ϵ	Heat exchanger effectiveness
μ	Dynamic viscosity ($Pa s$)
ρ	Density (Kg/m^3)
τ	Shear stress (Pa)

Subscripts

b	Bulk
c,i	Inlet of cold fluid
h,i	Inlet of hot fluid
i	Inner radial of tube side
w	Wall

vibration is an active method that is manipulated externally [6–8]. Any changes in heat exchanger configuration or geometry categorize in the passive method [9,10]. Nowadays, the combination of these methods is required to ensure optimized equipment [11–13]. Microtube Heat Exchangers (MTHXs), due to their well-organized and best-favorable process, have become a piece of efficient equipment in a wide range of industries such as electronic, heat pump, chemical engineering, HVAC system, cooling, refrigeration and solar systems [14–16]. A smaller distance for heat transfer, providing with MHXs, improves their performance compared to the traditional HXs. Plus, due to the miniature structure, the cost of manufacturing MHXs is economical since lower raw materials, initial investment, and working fluid are needed [17]. In some reactors in which reactions of hazard components have happened, utilizing MHXs is very useful in respect of safety because these HXs contain a lower material quantity [18]. In addition, this leads to reliable handling when an uncontrol incident occurred. Nowadays, various kinds of advanced MHXs are suggested by the researcher with changing their configuration. Applying a curve into the MHXs structure may transform the hydrothermal properties of the working fluid [19]. MHXs with C-, Y-, and S-shaped, L and T bend, spiral and helical coil, and coil flow inverter are the famous structures that have been proposed and studied more than others [20]. Helical HX has been chiefly utilized when heat transfer has occurred between two fluids that one of them includes a lower flow rate and higher temperature difference compared to another one. In this situation, a large heat transfer area is needed. So, helical HX finds it suitable to transfer the heat by single or double restrict but long tubes.

Regarding the tube's small surface area, it is designed for fluids with a low flow rate. Its long length is what causes the highest

temperature differences between inlet and outlet can be obtained. Followings are several usages of helical HXs:

- For limited space applications.
- For low fluid flow rate (laminar regime) as well as shell and tube HX has no economic efficiency due to its low heat transfer coefficients.
- For low pressure of one of the fluids through the HX.

Mir et al. [21] numerically analyzed the hydrodynamic characteristics of a curved mini channel with an oval cross-section. For this purpose, they used Ag/water nanofluid with volume concentrations up to 6%. They observed that the temperature of the central section of the mini channel would be augmented by raising the nanofluid concentration. Kannadasan et al. [22] experimentally studied a Helical coil HX in both vertical and horizontal situations while CuO/water nanofluid with 0.1 and 0.2 vol% was considered as working fluid. The findings indicated that the effect of nanofluid on hydrodynamic performance improvement of HX with vertical or horizontal situations is almost the same. Kurnia et al. [23] numerically explored the effect of various entrance shapes of a helical tube on heat transfer improvement. They considered helical tubes with square, circular, and elliptic, equal by the entrance of straight tubes. For all cases, the helical tubes had superior heat transfer performance compared to the straight tubes. Also, the tube with a square entrance showed the highest entropy generation relative to the others. Omidi et al. [24] modeled hydrodynamic specifications of a ribbed helical tube. They recognized the effect of the number of ribs on the tube and Reynolds number (Re) on heat transfer. They achieved that the higher the number of ribs, the lower the friction factor and the higher the Nusselt number (Nu). In addition, they used Al_2O_3 /water nanofluid and obtained 28% higher Nu than water, whereas the friction factor had no significant variation. In a comprehensive study, Rasheed et al. [5] investigated the effect of helical microtube HX with various entrance shapes, nanofluids, and nanofluid concentrations. They considered 1, 1.5, and 2 vol% concentrations of ZnO and Al_2O_3 nanoparticles in HX with elliptical, circle, and oval entrances. The results revealed that the helical path of fluid flow could increase the heat transfer compared to a straight one. Also, the highest heat transfer was observed for a circular tube entrance of HX for 2 vol% concentration of ZnO/water nanofluid. In Table 1, some studies on curved tubes are summarized.

Lately, the focus of studies is directed to HX with a helical double tube. As it was founded in other kinds of HXs, the first and second thermodynamic laws always rule on double tube one [33,34]. Like said conventional helical tube HXs, in this case, the geometrical effects on heat transfer and hydraulic characteristics have already been outstanding parameters for surveying. Majidi et al. [35] explored a helical double tube HX when the air was considered as working fluid. The novelty was copper fins attaching to the inner tube. The experiment results revealed the enhancement of heat transfer because of a new configuration. Eventually, they proposed a correlation for heat transfer coefficient in helical double-tube HX. Luo and Song [36] numerically examined the effect of twisted annulus placed between double oval pipes on the performance of a double-tube HX. The simulation results showed that a secondary flow is produced, which helps heat transfer improve by 157%. Koca and Citlak [37] experimentally investigated a double-tube HX in which the inner helical tube rotated. The observations indicated that the heat transfer enhances by rotating speed. Five rotating helixes tubes showed the most significant heat transfer improvement, up to 124.1%. In an exciting study, Alias et al. [18] conducted numerical

Table 1
Summary of researches about helical tubes heat transfer.

Author(s)	Study method	Configuration of HX	Working fluid	Achievements
Niu et al. [25]	Numerical	One-side heating helically coiled single tube	Water	Ununiform heating had lower heat transfer and pressure drop, compared to one-side heating
Alimoradi and Veysi [26]	Numerical and experimental	Shell & helical single tube HX	Water	34.1% and 2.83% shell side's Nu reduction is obtained by 50% diameter and height increment of the shell.
Alimoradi et al. [27]	Numerical	Shell & finned helical single tube HX	Water	Increasing the fin height and number enhances the heat transfer. The effect of the number of fins was more important than to their heights.
Zhang et al. [28]	Numerical	Shell & spherical finned helical single tube HX	Water	Increasing the fin height and pitch enhances the heat transfer up to 1.7 and 1.66 times while augmenting the friction factors by 1.24 and 1.28.
Mokhtari Ardekani et al. [29]	Experimental	Helical single tube	Ag/water SiO_2 /water	Ag and SiO_2 nanoparticles improved the heat transfer up to 45% and 50%, respectively.
Khoshvaght-Aliabadi et al. [30]	Experimental	MTHX	Cu/water	Coil diameter reduction enhanced Nu and friction factor. Adding Cu nanoparticles had no considerable effect on pressure drop. Maximum 2.24 times higher performance evaluation criterion was achieved by 0.3 vol% nanofluids.
Wei et al. [31]	Numerical	Circumferential corrugated helical tube	Al_2O_3 /water	The effect of nanoparticle volume fraction on friction factor was more than nanoparticle diameter. Nu was enhanced maximum of 31% by adding nanofluid concentration. Utilizing the novel system with nanofluid at the same time could raise the heat transfer performance by 29%.
Fouda et al. [32]	Numerical	Multi helical tube HX	Water	Heat transfer was improved by helical diameter and number of passing tubes. In comparison with single tubes, the multi tubes had 60% higher performance. Multi helical tube HX pumping power increased significantly, compared to single tube HX.

research on helical micro elliptical tube HX by considering water-based ZnO and SiO₂ nanofluids. The results showed that ZnO/water nanofluid has better heat transfer performance than SiO₂/H₂O. However, adding nanoparticles cause an enhancement in *Nu*, but it did not influence the friction factor. Rasheed et al. [38] numerically studied the heat transfer performance of a helical single microtube HX. The results indicated that the highest heat transfer could achieve by using a circular cross-section tube; the *Nu* of this structure was 3.42 times higher than the elliptical one. It was tried to report numerical or experimental studies about various types of HXs with single or double tubes, circle, square, or oval cross-section, micro or huge tube size. The most studies were focused on single helical tubes in a shell as shell and tube heat exchanger or single spiral tubes in microscale size. In contrast, the double-tube heat exchanger in microscale has not been studied yet.

However, this study investigated the helical micro double-tube heat exchanger's heat transfer performance and fluid flow (HMDTHX). Since this kind of HX has high industry applicability, an attempt was made to assess the heat transfer performance, pressure drop, pumping power, and fluid flow distribution in HMDTHX. For this purpose, the results were fulfilled at different Reynolds numbers. The achievement of this study can be helpful for electronic industry and scale-up processes, defense technology, frontier technology, and space.

2. Model description

2.1. Physical model

The computational domain included a helical micro double-tube heat exchanger (HMDTHX) which its isometric schematic is displayed in Fig. 1a. The length (*H*) of the straight tube was considered to be 30 mm, while, for helical cases, depends on pitch length (*P*), *H* and turns number (*n*) values were different. Also, the helical tube (*D*) diameter was maintained at 1.5 mm for all tested geometries. The inner diameter of the inner tube (*d_i*) and inner diameter of the outer tube (*d_o*) was the same for all simulated cases and equaled 250 μm and 450 μm, respectively. Outer tube thickness was considered negligible, whereas the thickness of the inner tube was 25 μm. Water was considered as working fluids of the tube and shell sides. Constant physicochemical properties of water are listed in Table 2. A schematic of half-cut HX for *P* = 1 mm is drawn in Fig. 1b.

In this study, 12 different micro double-tube HX have been configured which their *H*, *P*, and *n* values for various simulated cases are presented in Table 3.

2.2. Governing equations

Heat transfer performance, fluid flow characteristics, pumping power evaluation, and a geometric assessment of helical micro double-tube heat exchanger were determined by accomplishing 3-D numerical simulation utilizing ANSYS FLUENT software package. This software solves the following governing equations by using the finite volume method [40]:

Continuity equation:

$$\nabla \cdot (\vec{V}) = 0 \tag{1}$$

Momentum equation:

$$\rho (\vec{V} \nabla) \vec{V} = 0 \tag{2}$$

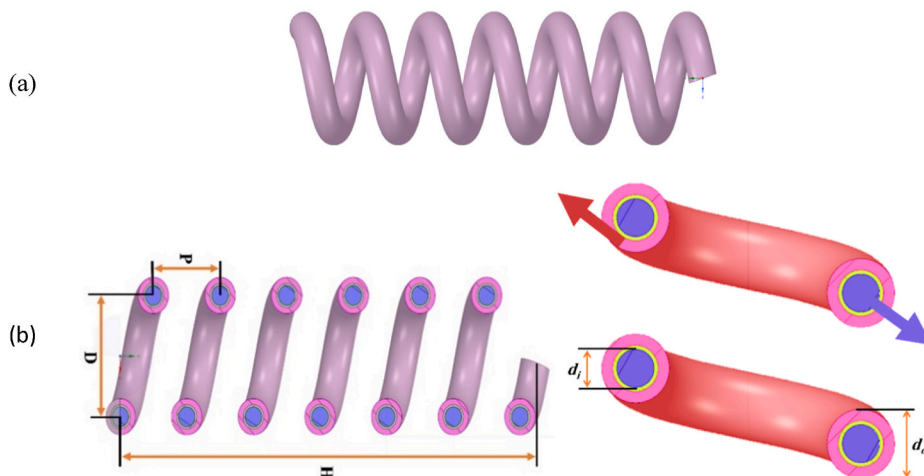


Fig. 1. (a) Isometric schematic of HMDTHX and (b) Schematic of half-cut HMDTHX with *P* = 1 mm.

Table 2
Specifications of water [39].

Density (kg/m ³)	Viscosity (Pa s)	Conductivity (W/m K)	Heat Capacity (J/kg K)
997.1	8.91×10^{-4}	0.6	4179

Table 3
Various sizes of HMDTHX configurations.

P (mm)	0.5	1	2	3	4	6	8	12	17	23	30	30
n	6.3307	6.2275	5.8602	5.3703	4.8535	3.9322	3.2311	2.327	1.7006	1.2778	0.9879	0
H (mm)	3.1653	6.2275	11.7205	16.1109	19.4139	23.5932	25.8488	27.924	28.9098	29.3895	29.6366	30

Energy equation:

$$\rho C_p (\vec{V} \cdot \nabla) T = k \nabla^2 T \quad (3)$$

The heat received by water (Q_{abs}) is defined by

$$Q_{abs} = \dot{m} C_p (T_o - T_i) \quad (4)$$

Convective heat transfer coefficient is obtained by

$$h = \frac{Q_{abs}}{A (\bar{T}_w - T_b)} \quad (5)$$

The friction factor would be calculated by

$$f = \frac{2\Delta P}{\rho V^2 \frac{L}{d_i}} \quad (6)$$

where ΔP is the pressure difference between outlet and inlet which is extracted via CFD.

The effectiveness of HMDTHX (ϵ) are defined as follows:

$$\epsilon = \frac{q}{q_{max}} = C_{min} (T_{h,i} - T_{c,i}) \quad (7)$$

where C_{min} is the minimum water's heat capacity between hot and cold flows.

Pumping power has been calculated by:

$$P_p = \dot{V} \Delta P \quad (8)$$

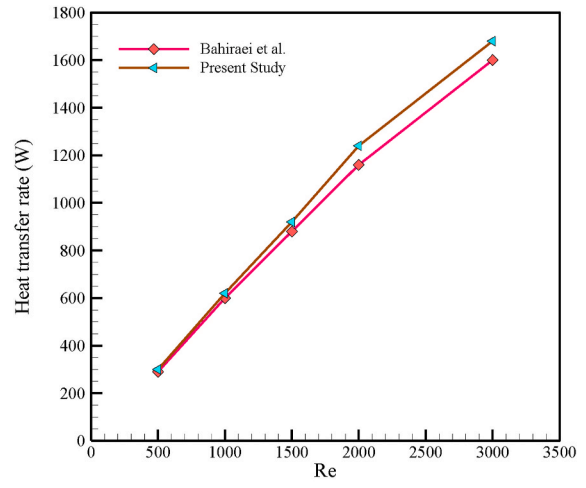
2.3. Boundary conditions

The modeling was simplified by applying the following boundary conditions on the HMDTHX system:

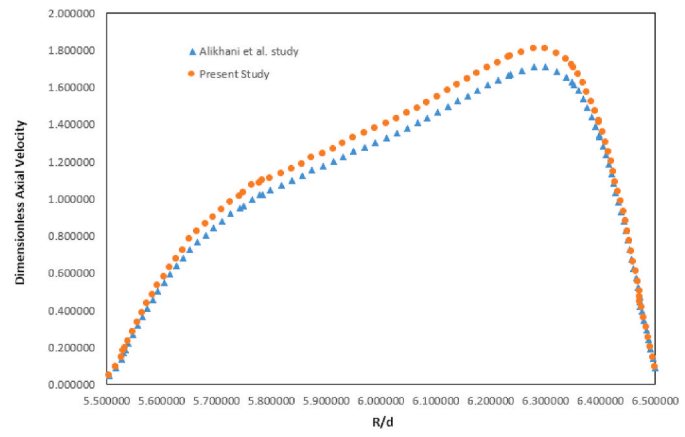
- Negligible gravity force.
- Newtonian behavior of water for both shell and tube sides.
- Incompressible, steady-state, laminar, and fully-developed conditions for working fluids flow.
- Counter-current fluid through the HX.
- Considering tube side inlet temperature of 300 K and shell side inlet temperature of 350 K.
- Constant Reynolds number of 50 for shell side and Reynolds numbers of 50, 100, 150, and 200 for tube side.
- Zero partial pressure at the outlet of tube and shell sides.
- No-slip boundary conditions on all walls.
- Adiabatic condition on the outer wall of the shell.
- Applying coupled boundary conditions on the joint walls between fluid and solid.

3. Numerical method

The finite volume method (FVM) through ANSYS FLUENT software package was utilized to solve the governing equations [41]. The Second-order upwind scheme [42] was employed all equations' discretization, whereas the SIMPLE algorithm [43] was utilized for the coupling of pressure and velocity. The convergence criteria for all governing equations were set equal to 10^{-9} to assure the accuracy of the calculations [44].



(a)



(b)

Fig. 2. Validation between the present study and (a) Bahiraei et al. [45] and (b) Alikhani et al. [32].

4. Validation

The model is validated by comparing the heat transfer rate data at various Reynolds numbers of present modeling and Bahiraei et al. [45]. A spiral HX was modeled in that study with a length and diameter of 30 cm and 10 cm, respectively. Coldwater and hot water or nanofluid flow through two sides of HX as counter-current with 280 K and 320 K temperatures, respectively. Uniform

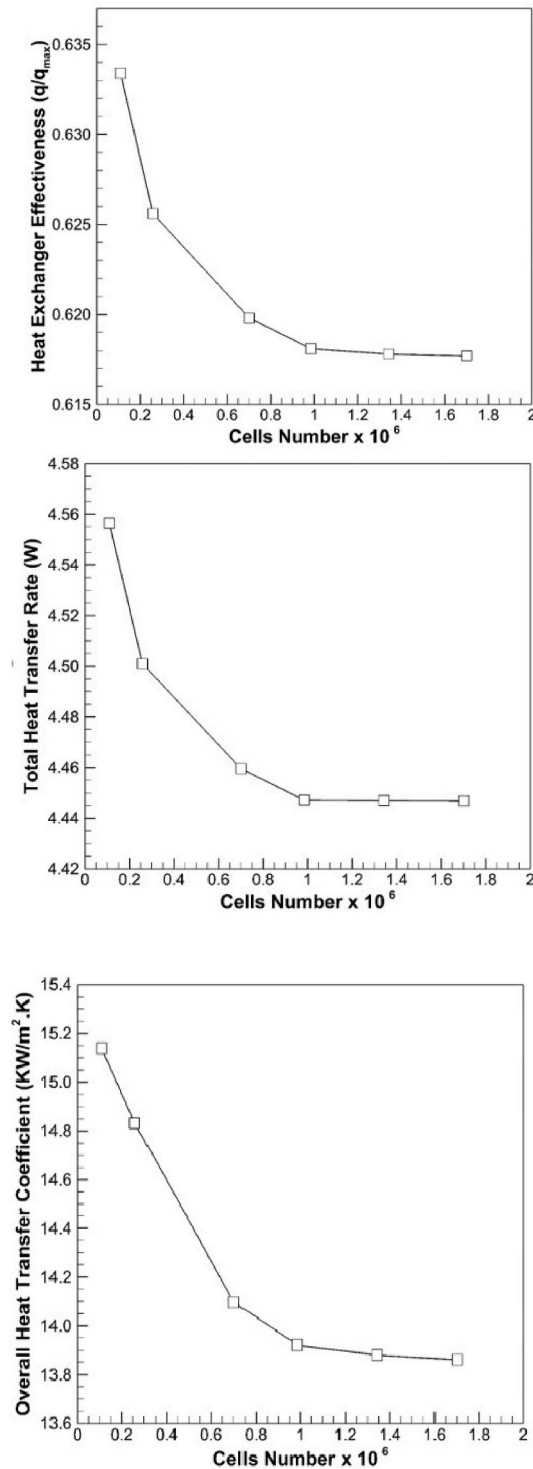


Fig. 3. Simulation performance at various cell numbers.

temperature and velocity, the insulated walls with no-slip conditions were boundary conditions. The results were reported as a function of Re which varied from 500 to 3000 with a step size of 500. As shown in Fig. 2a, a very well agreement is obtained from the present modeling and those reported by Bahiraei at all ranges of Re . At low Re , the difference is negligible, and at high Re , the maximum disagreement is less than 5%.

In another validation test, the fluid flow modeling of the present study was validated by the work of Alikhani et al. [46]. They have modeled a curved tube in which the Al_2O_3/H_2O nanofluid followed in the laminar regime at Reynolds number of 300, and two Grashof numbers of 100,000 and 500,000. In addition, the mixture method was used for mathematical modeling. The fluid flow of the present study and Alikhani et al. [46] are compared in Fig. 2b. In this figure, the dimensionless velocity at the axial line of the helical tube is presented against horizontal and vertical diameters. It is evident that the performed modeling has a very well resolution. Full compliance is observed at the inner zone of the tube, while a maximum of 5.6% deviation is calculated at the velocity peak zone, which is at the outer area of helical tube.

5. Grid independence analysis

Six examined different meshes for HMDTHX with a pitch length of 0.5 mm and Reynolds number of 200. It was the most sophisticated condition because the geometry curvature is at the highest value, so the flow gradients have the most complexation. Fig. 3 exhibits the performance of simulation on the hydrodynamic characteristics. As it is clear, increasing the cell number reduces each value of characteristics. However, after cell number 985,022, the performances have not considerable variance. This is the reason that cell numbers 985,022 have executed the all-cases simulations.

A schematic of meshed HMDTHX with $P = 1$ mm is indicated in Fig. 4. As can be seen from the figure, the most regular meshes are produced with 985,022 cells.

6. Results and discussion

The result of simulating the helical micro double-tube heat exchanger (HMDTHX) for hydrothermal performance is presented. The outcomes are carried out with dimensionless parameters, which means the parameters are presented based on their values compared to the straight HX.

Fig. 5 states the dimensionless overall heat transfer coefficient (OHTC) against pitch length (P) for different Reynolds numbers (Re) of the inner tube. As is expected, increasing the values of Re leads to OHTC enhancement induced by increasing the fluid distribution. So, fresh fluid replaces with an old one, the repetition of this procedure would enhance OHTC. It causes 17.5% OHTC enhancement by rising Re from 50 to 200. It is clear that by creating even a small turn in the straight HX, OHTC increases. What is clear is that the lower the pitch length, the higher the heat transfer coefficient. However, HMDTHX with minimal P values have not the performance of $P = 2$

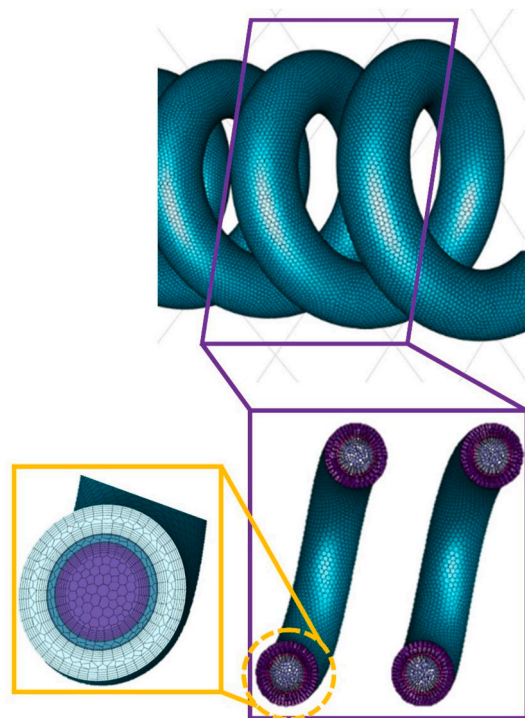


Fig. 4. The meshes of micro helical double tube heat exchanger with $P = 1$ mm.

mm. The highest OHTC is achieved for turn number (n) of 5.8602, which had almost 45% heat transfer enhancement at Re = 200, compared to the straight HX. At this point, the maximum OHTC enhancement is achieved, while further pinch lengths reduce the performance of HX. From n = 4.8535 to n = 1.7006, as Re increases, the heat transfer falling will accelerate. Higher turn number leads to an efficient contact area which donates this opportunity to the heat energy between working fluids through shell and tube to exchange more effectively. It is clear that at high Reynolds numbers, maximum OHTC is obtained for P = 2. However, for Re = 50, OHTC value at P = 1 is maximum. One thing that should be noted from the figure is at a certain Re, OHTC enhancement for HX with P = 29 and P = 30 (with almost one swirl) is negligible, while by decreasing P, the slop of the enhancement is augmented. Practically, the centrifugal force of working fluid resulted from the helical path can affect the heat transfer coefficient. This force is insignificant at high pitch lengths, but decreasing the pitch length (P) amplifies that. Thus, at high pitch lengths, rising Re slightly increases OHTC, whereas, at low pitch lengths, it significantly increases OHTC, as the centrifugal force at lower P (higher swirl) is more sensible.

In Fig. 6, dimensionless inner tube wall heat flux versus pitch length (P) for various Re is demonstrated. Similar to the trends of Fig. 5, heat flux, at first, increases by P, then it sharply decreases. Increasing P, or torsion, in other words, the helical double tube becomes similar to straight tubes with low n values. Hence, the fluctuation of axial velocity, which is affected by the centrifugal force, lessens. For all cases, the heat flux is higher than straight HX. For all Reynolds numbers, maximum heat flux in the inner tube is achieved at P = 3 (n = 5.3703). 12.5% higher heat flux at the inner tube wall is achieved by an HX with a pitch length of 3 at Re = 200. The centrifugal forces will augment firstly, then weaken by elevating P, as the torsion effects will grow at first and then reduce. This issue affects the velocity component and dwindles its rate. As an outcome for P > 3, the maximum values of axial velocity will include displacement from the outer curvature area to the inner curvature. Finally, this displacement gradually is dispelled, and the velocity role gets closer to its behavior in a straight tube [47]. Therefore, the exchanged heat due to the distribution of fluid flow components decreases, and heat flux will reduce.

Using equation (7), dimensionless heat exchanger effectiveness is depicted in Fig. 7 as a function of pitch length at different Reynolds numbers of the inner tube. As it is obvious, the effectiveness of HX, in general, is diminished. However, it has different maximum points at each Re. For Re = 50, with a maximum at P = 3 (n = 5.3703), the effectiveness is reduced by P. Whereas, at Re = 100, the maximum effectiveness is calculated at P = 1. Also, for Re = 150 and 200, the maximum values are at P = 2. The maximum heat exchanger effectiveness is 11.5%. Although OHTC of Re = 50 was 1.27 (27% enhancement by reducing P), the heat exchanger effectiveness and heat flux were enhanced by a maximum of 2.7%. At Re = 100, a slight rising in the effectiveness is seen at lower P, and then the reduction trend began. This trend is not observed for the heat flux and OHTC of Re = 100, while a similar procedure is seen for OHTC at Re = 50. Increasing the effectiveness would be because of OHTC enhancement. It leads to a higher heat transfer rate.

Fig. 8(a) and (b) represent dimensionless pressure drop and shear stress for the inner tube wall against pitch length for various Reynolds numbers. As is expected from the equation $\tau = \mu V/r$, the shear stress augments by fluid velocity. So, from the figure, by increasing Re, the shear stress enhances by P, except at Re = 50, a maximum observed at P = 2. At the same time, the pressure drop reduction trend of the inner tube at all Reynolds numbers is accompanied by a maximum at P = 2 for Re = 50 and P = 3 for the rest. Thus, the maximum pressure drop is obtained at Re = 200, 42% more than the straight tube. Strong secondary flow will be the result of applying a helix angle into the tube. Increasing the turn numbers causes a more robust secondary flow. Because of the curvature effect, the fluid contacts the tube wall. This effect gets significant when the turn number increases. Nevertheless, this effect has a limit point: it has different values at different Reynolds numbers. However, it can be said that the length numbers of 2 and 3 are the limit points.

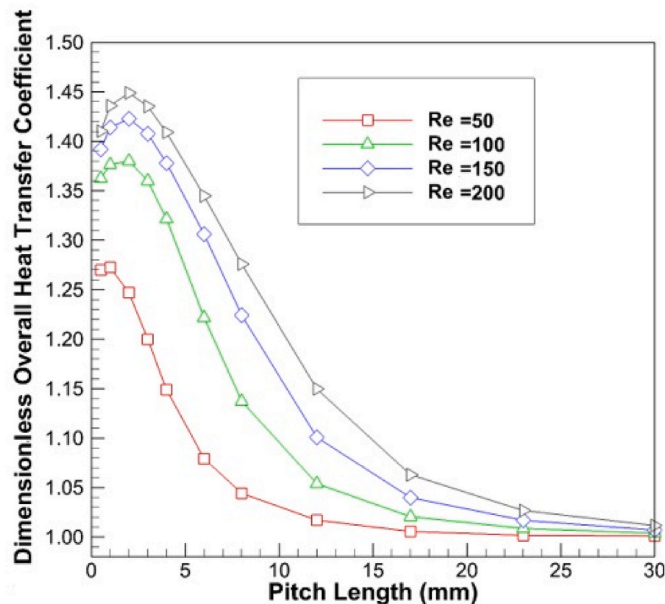


Fig. 5. Dimensionless overall heat transfer coefficient vs. pitch length.

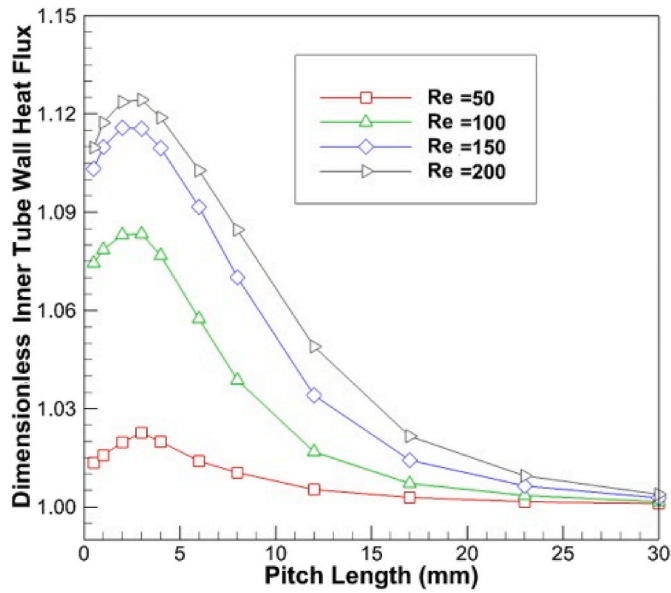


Fig. 6. Dimensionless inner tube wall heat flux vs. pitch length.

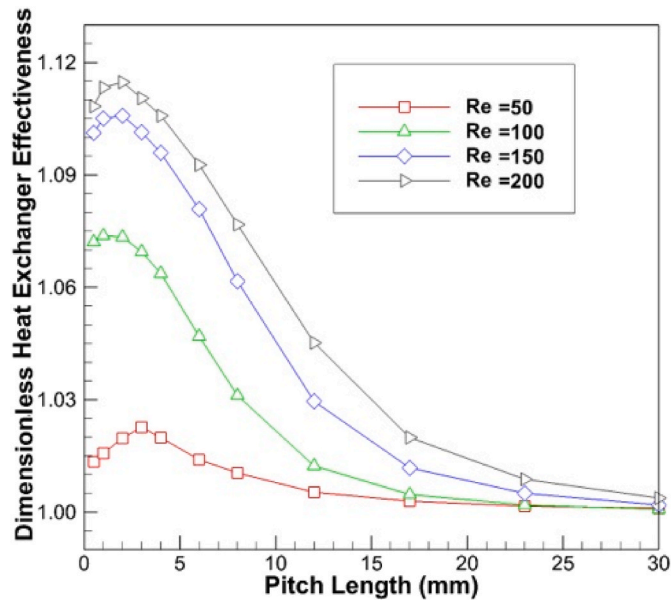


Fig. 7. Dimensionless heat exchanger effectiveness vs. pitch length.

The pumping power and friction factor of the inner helical tube are shown in Fig. 9(a) and (b). As can be seen from the figures, the trends of friction factor and pumping power are similar to the pressure drop trend because they are proportional to the pressure drop quantity. The pumping power and friction factor reduce by P , although it has a maximum value at $P = 2$ for $Re = 50$ and $P = 3$ for all other studied cases. Generally, friction factor augments with Re . It is because of pressure drop rising, which is induced by velocity gradient. Pumping power at $Re = 200$ is 31% higher than $Re = 50$, at maximum points. While, by increasing the P , the pumping powers decrease. $P \geq 17$ at a certain Re , pumping power, and friction factor have no remarkable difference compared to the straight tube. Maximum pumping power and friction factor are 42% in comparison with the straight tube.

Temperature and velocity distributions are displayed in Fig. 10. Temperature distributions through the tube and shell sides of straight HX at $Re = 200$ are illustrated in Fig. 10a. The tube side inlet is at the left, and its temperature is 300 K. Also, the shell side inlet is at the right and at 350 K. The average outlet temperature of tube side fluid reaches 327.9 K, whereas, at the tube wall, the temperature is 343 K. Moreover, the average outlet temperature of shell-side fluid reaches 313.3 K. In Fig. 10b, the velocity contour of the

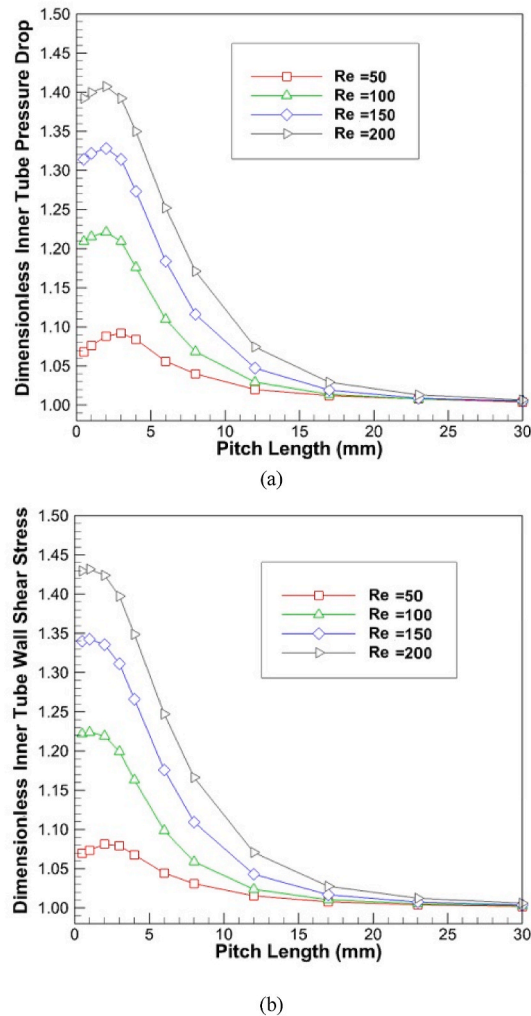


Fig. 8. Dimensionless inner tube wall a) pressure drop and b) shear stress vs. pitch length.

tube side of straight HX for $Re = 200$ is depicted. At the inlet, the uniform velocity is equal to 0.7149 m/s. In the figure, the fully-developed length is observed. It is evident from the figure that this length is negligible compared to the whole tube length. Therefore, it cannot be expected to have a high heat transfer rate from this flow distribution. Fig. 10c demonstrates the temperature distribution of the tube side's wall of helical HX for $Re = 200$. Like the straight tube, in helical HX, the maximum temperature on the tube wall is 343 K. But the point is the average outlet temperature which reaches 331.1 K; 3.2 K higher than the straight tube. More heat energy is received from the tube wall through the flow path by applying a helix angle in the tube. The reason for this phenomenon can be surveyed by looking into the velocity distribution through the tube's fluid flow. The velocity contour of fluid flow in the tube side of helical HX for a vertical cross-sectional profile is displayed in Fig. 10d. It can be seen from the figure that a secondary flow is formed through the tube. It has a low-pressure zone with high velocity near the tube's outer curvature because centrifugal forces push the fluid flow to the outside of the force effect line. Also, a high-pressure zone with low fluid velocity is found in the tube's inner curvature. The interaction between these two zones creates secondary flow. It causes higher turbulency, consequently higher heat transfer rate, and pressure drop. Therefore, it was investigated that helical HX has higher heat transfer performance compared to a straight one. In this study, 12 different micro double-tube HX have been explored. However, it can be concluded that an increase in turn number or reducing pitch length in constant tube length has an optimum point which is between $n = 6.2275$ and 5.3703 or $P = 1$ to 3 . Besides this optimum point, the helical HX performance decreases.

7. Conclusion

Hydrothermal characteristics of a helical micro double-tube heat exchanger (HMDTHX) were numerically investigated. There were considered 12 various HMDTHX configurations to be tested. Pitch length (P) was chosen between 0.5 mm and 30 mm, turn number varied from 6.3307 to 0.9879, so the height of HMDTHX differed from 3.1653 mm to 29.3895 mm to remain the whole heat exchanger

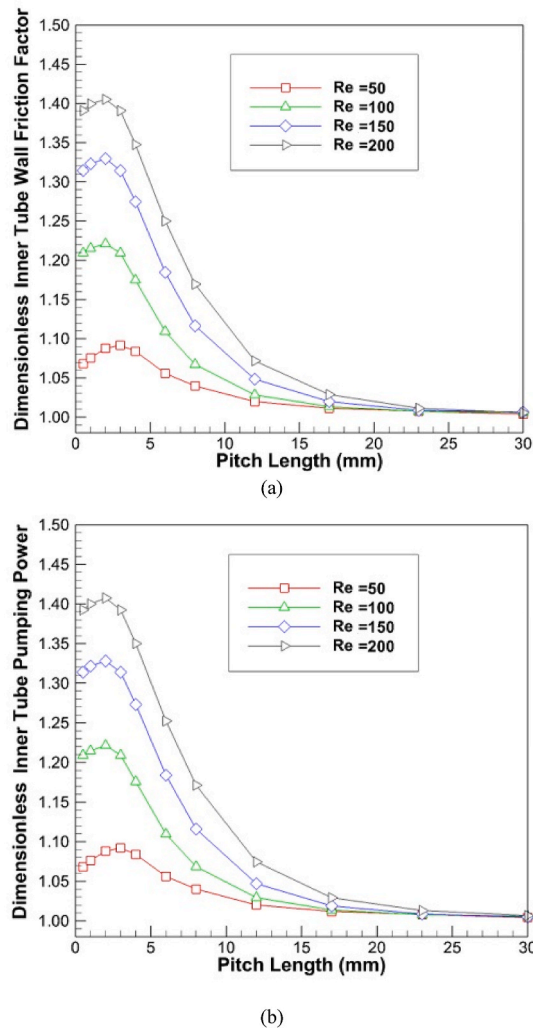


Fig. 9. Dimensionless inner tube a) friction factor and b) pumping power vs. pitch length.

length at 30 mm. In addition, the results were reported for Reynolds numbers (Re) of 50, 100, 150, and 200. All HMDTHX had better performance in comparison with straight heat exchangers. The main results are as follow:

- Overall heat transfer coefficient (OHTC) enhanced by Re, while it reduced by P with a maximum at $P = 2$ for $Re = 100$ to 200 and $P = 1$ for $Re = 50$. The maximum OHTC enhancement was obtained at $P = 2$ for $Re = 200$, which was almost 45% compared to the straight double tube HX. The centrifugal force made by swirl was the reason for this enhancement.
- Heat flux at the inner tube wall had a maximum value at $P = 3$ for all Re, which was 12.5%, at the maximum Re, higher than the straight tube.
- Heat exchanger effectiveness was increased by Re and decreased by P with a maximum at $P = 3, 1, 2,$ and 2 for $Re = 50, 100, 150,$ and $200,$ respectively. Maximum effectiveness was 11.5% for $P = 2$ and $Re = 200$.
- Shear stress for $Re = 100$ to 200 are almost the same for $P = 0.5$ and 1 . Then by increasing P, the shear stress decreases. While, for $Re = 50$, a maximum is seen at $P = 2$.
- Pressure drop, friction factor, and pumping power changes were the same. They augmented by Re and reduced by P with a maximum at $P = 2$ for $Re = 100$ to 200 and $P = 3$ for $Re = 50$. The maximum pressure drop, pumping power, and friction factor were 42%, compared to the straight double tube HX.
- Velocity contour revealed a secondary flow through the HMDTHX, which is why the existing centrifugal force.
- The outlet temperature of HMDTHX at $Re = 200$ is 331.1 K which was 3.2 K higher than the straight HX.

Author contributions

Conceptualization, N.H.A.H., M.G.; methodology, R.A.A., N.H.A.H.; software, A.A.A., H.F.S.; validation, M.A.A., M.A.E.; formal

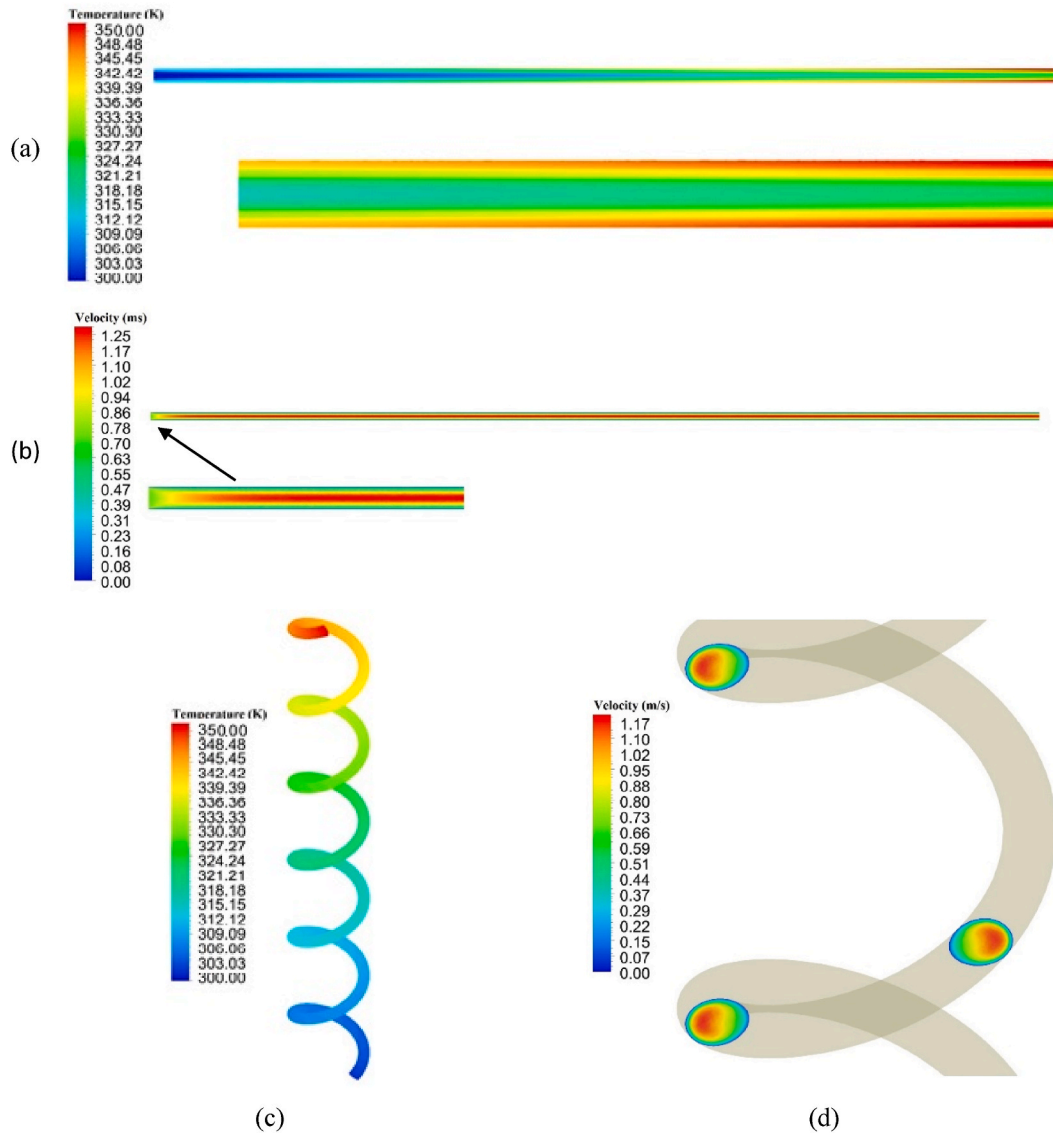


Fig. 10. (a) Temperature distribution at shell and tube sides of straight HX at $Re = 200$, (b) Velocity contour of tube side of straight HX for $Re = 200$, (c) Temperature distribution of tube side's wall of helical HX for $Re = 200$, and (d) Velocity contour of tube side of helical HX for $Re = 200$.

analysis, K.A.A., M.A.E.; investigation, R.A.A., H.F.S.; resources, M.A.A., K.H.A.; visualization, A.A.A., K.H.A.; data curation, K.A.A., M. J.H.R.; writing—original draft preparation, M.G., M.R.S.; writing—review and editing, A.M.A., M.J.H.R.; supervision, M.G., M.R.S.; project administration, M.G., N.H.A.H.; funding acquisition, M.R.S., N.H.A.H. All authors have read and agreed to the published version of the manuscript.

Declaration of competing interest

The authors declare that there is no conflict of interest regarding the publication of this paper.

Acknowledgment

This research work was funded by Institutional Fund Projects under grant no. (IFPNC-006-135-2020). Therefore, the authors gratefully acknowledge technical and financial support from the Ministry of Education and King Abdulaziz University, Jeddah, Saudi Arabia.

References

- [1] M.R. Saffarian, M. Moravej, M.H. Doranehgard, Heat transfer enhancement in a flat plate solar collector with different flow path shapes using nanofluid, *Renew. Energy* 146 (2020) 2316–2329.
- [2] M. Sarafraz, M.R. Safaei, Diurnal thermal evaluation of an evacuated tube solar collector (ETSC) charged with graphene nanoplatelets-methanol nano-suspension, *Renew. Energy* 142 (2019) 364–372.
- [3] M.H. Doranehgard, H. Dehghanpour, Quantification of convective and diffusive transport during CO₂ dissolution in oil: a numerical and analytical study, *Phys. Fluids* 32 (8) (2020), 085110.
- [4] M. Hossein Doranehgard, S. Tran, H. Dehghanpour, Modeling of natural-gas diffusion in oil-saturated tight porous media, *Fuel* 300 (2021), 120999.
- [5] A. Sohani, H. Sayyaadi, M.H. Doranehgard, S. Nizetic, L.K.B. Li, A method for improving the accuracy of numerical simulations of a photovoltaic panel, *Sustainable Energy Technologies and Assessments* 47 (2021) 101433.
- [6] M.A. Alazwari, M.R. Safaei, Non-isothermal hydrodynamic characteristics of a nanofluid in a fin-attached rotating tube bundle, *Mathematics* 9 (10) (2021) 1153.
- [7] S. Nazari, R. Ellahi, M. Sarafraz, M.R. Safaei, A. Asgari, O.A. Akbari, Numerical study on mixed convection of a non-Newtonian nanofluid with porous media in a two lid-driven square cavity, *J. Therm. Anal. Calorim.* 140 (3) (2020) 1121–1145.
- [8] M. Nakhjavani, V. Nikkhah, M. Sarafraz, S. Shoja, M. Sarafraz, Green synthesis of silver nanoparticles using green tea leaves: experimental study on the morphological, rheological and antibacterial behaviour, *Heat Mass Tran.* 53 (10) (2017) 3201–3209.
- [9] M.A. Alazwari, M.R. Safaei, Combination effect of baffle arrangement and hybrid nanofluid on thermal performance of a shell and tube heat exchanger using 3-D homogeneous mixture model, *Mathematics* 9 (8) (2021) 881.
- [10] M. Sarafraz, F. Hormozi, Heat transfer, pressure drop and fouling studies of multi-walled carbon nanotube nano-fluids inside a plate heat exchanger, *Exp. Therm. Fluid Sci.* 72 (2016) 1–11.
- [11] M. Sarafraz, T. Kiani, F. Hormozi, Critical heat flux and pool boiling heat transfer analysis of synthesized zirconia aqueous nano-fluids, *Int. Commun. Heat Mass Tran.* 70 (2016) 75–83.
- [12] M. Sarafraz, F. Hormozi, V. Nikkhah, Thermal performance of a counter-current double pipe heat exchanger working with COOH-CNT/water nanofluids, *Exp. Therm. Fluid Sci.* 78 (2016) 41–49.
- [13] V. Nikkhah, M. Sarafraz, F. Hormozi, Application of spherical copper oxide (II) water nano-fluid as a potential coolant in a boiling annular heat exchanger, *Chem. Biochem. Eng. Q.* 29 (3) (2015) 405–415.
- [14] M. Sarafraz, M. Arjomandi, Thermal performance analysis of a microchannel heat sink cooling with copper oxide-indium (CuO/In) nano-suspensions at high-temperatures, *Appl. Therm. Eng.* 137 (2018) 700–709.
- [15] M. Goodarzi, I. Tlili, Z. Tian, M.R. Safaei, Efficiency assessment of using graphene nanoplatelets-silver/water nanofluids in microchannel heat sinks with different cross-sections for electronics cooling, *International Journal of Numerical Methods for Heat & Fluid Flow*, 2019.
- [16] M. Sarafraz, A. Arya, F. Hormozi, V. Nikkhah, On the convective thermal performance of a CPU cooler working with liquid gallium and CuO/water nanofluid: a comparative study, *Appl. Therm. Eng.* 112 (2017) 1373–1381.
- [17] M. Sarafraz, M.R. Safaei, M. Goodarzi, B. Yang, M. Arjomandi, Heat transfer analysis of Ga-In-Sn in a compact heat exchanger equipped with straight micro-passages, *Int. J. Heat Mass Tran.* 139 (2019) 675–684.
- [18] M. Sarafraz, M.R. Safaei, M. Goodarzi, M. Arjomandi, Reforming of methanol with steam in a micro-reactor with Cu–SiO₂ porous catalyst, *Int. J. Hydrogen Energy* 44 (36) (2019) 19628–19639.
- [19] O.A. Akbari, M.R. Safaei, M. Goodarzi, N.S. Akbar, M. Zarringhalam, G.A.S. Shabani, M. Dahari, A modified two-phase mixture model of nanofluid flow and heat transfer in a 3-D curved microtube, *Adv. Powder Technol.* 27 (5) (2016) 2175–2185.
- [20] Z. Tian, A. Abdollahi, M. Shariati, A. Amindoust, H. Arasteh, A. Karimipour, M. Goodarzi, Q.-V. Bach, Turbulent flows in a spiral double-pipe heat exchanger: optimal performance conditions using an enhanced genetic algorithm, *International Journal of Numerical Methods for Heat & Fluid Flow*, 2019.
- [21] S. Mir, O.A. Akbari, D. Toghraie, G. Sheikhzadeh, A. Marzban, S. Mir, P. Talebizadehsardari, A comprehensive study of two-phase flow and heat transfer of water/Ag nanofluid in an elliptical curved minichannel, *Chin. J. Chem. Eng.* 28 (2) (2020) 383–402.
- [22] N. Kannadasan, K. Ramanathan, S. Suresh, Comparison of heat transfer and pressure drop in horizontal and vertical helically coiled heat exchanger with CuO/water based nano fluids, *Exp. Therm. Fluid Sci.* 42 (2012) 64–70.
- [23] J.C. Kurnia, A.P. Sasmito, T. Shamim, A.S. Mujumdar, Numerical investigation of heat transfer and entropy generation of laminar flow in helical tubes with various cross sections, *Appl. Therm. Eng.* 102 (2016) 849–860.
- [24] M. Omid, M. Farhadi, A. Ali Rabienataj Darzi, Numerical study of heat transfer on using lobed cross sections in helical coil heat exchangers: effect of physical and geometrical parameters, *Energy Convers. Manag.* 176 (2018) 236–245.
- [25] X. Niu, S. Luo, L.-L. Fan, L. Zhao, Numerical simulation on the flow and heat transfer characteristics in the one-side heating helically coiled tubes, *Appl. Therm. Eng.* 106 (2016) 579–587.
- [26] A. Alimoradi, F. Veysi, Prediction of heat transfer coefficients of shell and coiled tube heat exchangers using numerical method and experimental validation, *Int. J. Therm. Sci.* 107 (2016) 196–208.
- [27] A. Alimoradi, M. Olfati, M. Maghareh, Numerical investigation of heat transfer intensification in shell and helically coiled finned tube heat exchangers and design optimization, *Chem. Eng. Process: Process Intensification* 121 (2017) 125–143.
- [28] C. Zhang, D. Wang, S. Xiang, Y. Han, X. Peng, Numerical investigation of heat transfer and pressure drop in helically coiled tube with spherical corrugation, *Int. J. Heat Mass Tran.* 113 (2017) 332–341.
- [29] A. Mokhtari Ardekani, V. Kalantar, M.M. Heyhat, Experimental study on heat transfer enhancement of nanofluid flow through helical tubes, *Adv. Powder Technol.* 30 (9) (2019) 1815–1822.
- [30] M. Khoshvaght-Aliabadi, S. Pazdar, O. Sartipzadeh, Experimental investigation of water based nanofluid containing copper nanoparticles across helical microtubes, *Int. Commun. Heat Mass Tran.* 70 (2016) 84–92.
- [31] H. Wei, H. Moria, K.S. Nisar, R. Ghandour, A. Issakhov, Y.-L. Sun, A. Kaood, M.M. Youshanlouei, Effect of volume fraction and size of Al₂O₃ nanoparticles in thermal, frictional and economic performance of circumferential corrugated helical tube, *Case Studies in Thermal Engineering* 25 (2021) 100948.
- [32] A. Fouda, S.A. Nada, H.F. Elattar, H.A. Refaey, A.S. Bin-Mahfouz, Thermal performance modeling of turbulent flow in multi tube in tube helically coiled heat exchangers, *Int. J. Mech. Sci.* 135 (2018) 621–638.
- [33] J. Wang, S.S. Hashemi, S. Alahgholi, M. Mehri, M. Safarzadeh, A. Alimoradi, Analysis of Exergy and energy in shell and helically coiled finned tube heat exchangers and design optimization, *Int. J. Refrig.* 94 (2018) 11–23.
- [34] S.-R. Yan, H. Moria, S. Pourhedayat, M. Hashemian, S. Asaadi, H. Sadighi Dizaji, K. Jermisittiparsert, A critique of effectiveness concept for heat exchangers; theoretical-experimental study, *Int. J. Heat Mass Tran.* 159 (2020) 120160.
- [35] D. Majidi, H. Alighardashi, F. Farhadi, Experimental studies of heat transfer of air in a double-pipe helical heat exchanger, *Appl. Therm. Eng.* 133 (2018) 276–282.
- [36] C. Luo, K. Song, Thermal performance enhancement of a double-tube heat exchanger with novel twisted annulus formed by counter-twisted oval tubes, *Int. J. Therm. Sci.* 164 (2021) 106892.
- [37] T. Koca, A. Çitlak, Design and analysis of double-pipe heat exchanger using both helical and rotating inner pipe, *Therm. Sci.* (2021) 66.
- [38] A.H. Rasheed, H.B. Alias, S.D. Salman, Numerical study of the heat transfer behavior in helical microcoil tube. *IOP Conference Series: Materials Science and Engineering*, IOP Publishing, 2020, 012014.
- [39] M. Goodarzi, M. Safaei, K. Vafai, G. Ahmadi, M. Dahari, S. Kazi, N. Jomhari, Investigation of nanofluid mixed convection in a shallow cavity using a two-phase mixture model, *Int. J. Therm. Sci.* 75 (2014) 204–220.

- [40] M.R. Safaei, M. Safdari Shadloo, M.S. Goodarzi, A. Hadjadj, H.R. Goshayeshi, M. Afrand, S. Kazi, A survey on experimental and numerical studies of convection heat transfer of nanofluids inside closed conduits, *Adv. Mech. Eng.* 8 (10) (2016), 1687814016673569.
- [41] T. Abdulrazzaq, H. Togun, H. Alsulami, M. Goodarzi, M.R. Safaei, Heat transfer improvement in a double backward-facing expanding channel using different working fluids, *Symmetry* 12 (7) (2020) 1088.
- [42] A.A. Ahmadi, M. Arabbeiki, H.M. Ali, M. Goodarzi, M.R. Safaei, Configuration and optimization of a minichannel using water–alumina nanofluid by non-dominated sorting genetic algorithm and response surface method, *Nanomaterials* 10 (5) (2020) 901.
- [43] H. Arasteh, R. Mashayekhi, M. Goodarzi, S.H. Motaharpour, M. Dahari, D. Toghraie, Heat and fluid flow analysis of metal foam embedded in a double-layered sinusoidal heat sink under local thermal non-equilibrium condition using nanofluid, *J. Therm. Anal. Calorim.* 138 (2) (2019) 1461–1476.
- [44] M. Safaei, H. Togun, K. Vafai, S. Kazi, A. Badarudin, Investigation of heat transfer enhancement in a forward-facing contracting channel using FMWCNT nanofluids, *Numer. Heat Tran., Part A: Applications* 66 (12) (2014) 1321–1340.
- [45] M. Bahiraei, H.K. Salmi, M.R. Safaei, Effect of employing a new biological nanofluid containing functionalized graphene nanoplatelets on thermal and hydraulic characteristics of a spiral heat exchanger, *Energy Convers. Manag.* 180 (2019) 72–82.
- [46] S. Alikhani, A. Behzadmehr, M. Saffar-Avval, Numerical study of nanofluid mixed convection in a horizontal curved tube using two-phase approach, *Heat Mass Tran.* 47 (1) (2011) 107–118.
- [47] M. Nobari, A. Malvandi, Torsion and curvature effects on fluid flow in a helical annulus, *Int. J. Non Lin. Mech.* 57 (2013) 90–101.